ACS Partner Journal

POLYMER SCIENCE & TECHNOLOGY

https://pubs.acs.org/PolySciTech

Article

Polymorphism in Self-Assembly of Short Peptoid Sequences

Renyu Zheng, Mingfei Zhao, Wenhao Zhou, Thi Kim Hoang Trinh, Shuai Zhang, James J. De Yoreo, Andrew L. Ferguson, and Chun-Long Chen*

Cite This: *Polym. Sci. Technol.* 2026, 2, 176−185

Read Online

ACCESS | Metrics & More | Article Recommendations | Supporting Information

ABSTRACT: Due to various applications enabled by diverse morphologies of self-assembled sequence-defined polymers, controlling the self-assembly of synthetic peptidomimetics into designed morphologies has emerged as a promising route for the development of bioinspired functional materials. Herein, we report morphological control over the assembly of a series of short peptoids, or poly-*N*-substituted glycines, that contain asymmetric hydrophobic domains. We demonstrate that the inherent flexibility of amphiphilic peptoid bilayers drives assembly polymorphism, resulting in the coexistence of nanosheets, twisted ribbons, and nanofibers—three distinct morphologies. By tuning peptoid molecular interactions through variations in sequence design, solution pH, and temperature, we demonstrate precise control over the twisting and folding of peptoid bilayers, enabling the formation of well-defined nanosheets and nanohelices. Molecular dynamics simulations further unravel how the introduction of asymmetric hydrophobic domains enables the flexibility of peptoid bilayers and results in peptoid assembly polymorphism. By tuning peptoid molecular interactions through heating, we further demonstrate the transformation of nanosheets into nanohelices. We envision that our mechanistic investigation of peptoid assembly polymorphism provides a strong foundation for leveraging peptoid sequences and chemistries to achieve controlled molecular interactions, driving the creation of biomimetic materials with tailored morphologies and functionalities.

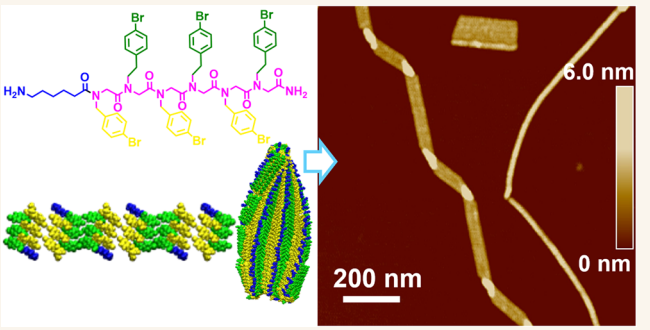

KEYWORDS: *sequence-defined polymers, peptoids, assembly polymorphism, morphological control, biomimetic materials*

INTRODUCTION

Living organisms use sequence-specific biomolecules like proteins and peptides to create sophisticated functional biomaterials.[1−5] To accomplish a wide range of crucial functions *in vivo*, these biomolecules need to go through specific changes in conformation and assembly morphology to reach their final supramolecular structures.[5−8] These processes, similar to the bottom-up self-assembly of synthetic macromolecules, are often dominated by noncovalent interactions, which include hydrophobic interactions (e.g., $\pi-\pi$ stacking), hydrogen bonding, van der Waals forces, and electrostatic interactions.[1,5,7,9] The assembly conditions, such as temperature, solution pH, concentration, and ionic strength, can significantly influence the outcome and pathway of macromolecular assembly processes.[5,9,10] Taken together, these molecular interactions can change the flexibility of assembled nanostructures from biopolymers or synthetic polymers, either in conformational flexibility[11,12] or in mechanical flexibility,[13,14] thereby resulting in assembly polymorphism. Therefore, identifying dominant interactions to achieve precise control over macromolecular assembly polymorphism through flexibility variation can significantly benefit the development of bioinspired functional materials and understanding their corresponding structure−function relationships.[5,15−17]

Peptoids, or poly-*N*-substituted glycines, are sequence-defined synthetic macromolecules that mimic the structure of peptides by having side-chain groups on nitrogen instead of α-carbon positions. These macromolecules retain the sequence-programmability and side-chain diversity inherited from peptides but lack backbone hydrogen bond donors and chirality.[5,9,18,19] Therefore, peptoid−peptoid and peptoid−substrate interactions can be controlled by varying the side-chain chemistry for the development of functional materials.[5,9,15,20,21] Amphiphilic peptoids have been designed and synthesized to assemble functional materials with diverse morphologies, including nanotubes,[22−26] nanosheets,[25−36] and nanohelices.[37,38] While significant progress has been made in unraveling the molecular interactions that govern peptoid assemblies and transitions among these nanostructures,[39−41]

Received: October 20, 2025
Revised: January 19, 2026
Accepted: January 19, 2026
Published: January 30, 2026

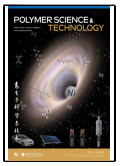

https://doi.org/10.1021/polymscitech.5c00123
Polym. Sci. Technol. 2026, 2, 176−185

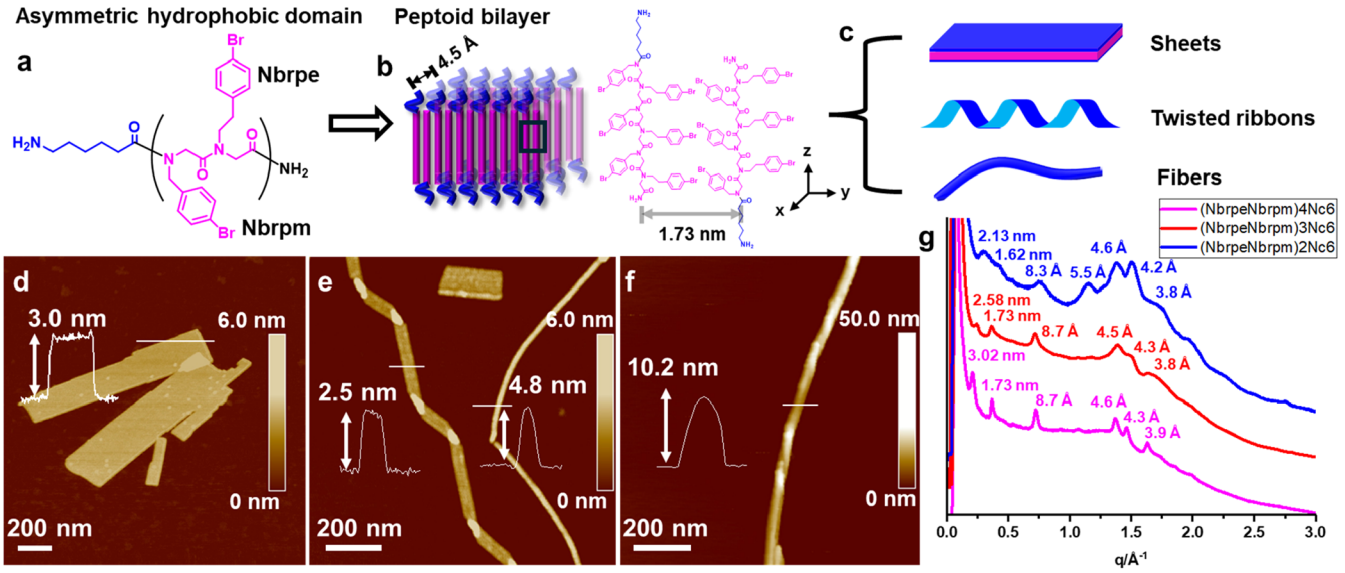

Figure 1. Self-assembly of peptoid sequences with asymmetric hydrophobic domains. (a) Structures of $(NbrpeNbrpm)_nNc_6$ (n = 2, 3, and 4). (b) Schematic illustrating the interdigitated peptoid bilayer structure with molecular packing distances identified from XRD peaks. (c) Flexibility of the peptoid bilayer promotes self-assembly into various morphologies, such as nanosheets, twisted ribbons, and helical fibers. (d–f) AFM images of various morphologies of peptoid assemblies: (d) Nanosheets from $(NbrpeNbrpm)_4Nc_6$; (e) coexistence of nanosheets, twisted ribbons, and fibers from $(NbrpeNbrpm)_3Nc_6$; and (f) helical fibers from $(NbrpeNbrpm)_2Nc_6$. (g) XRD spectra of the assembled materials from $(NbrpeNbrpm)_nNc_6$.

precisely controlling these interactions to achieve specific morphologies remains a challenging task.

Herein, we present controlled supramolecular polymorphism in the assembly of a series of short amphiphilic peptoids featuring asymmetric hydrophobic domains. We demonstrate that these peptoid sequences self-assemble into defined nanostructures, including nanosheets, twisted nanoribbons, and nanohelices, by modulating their molecular interactions through variations in the hydrophobic domain length and assembly conditions. Molecular dynamics (MD) simulations reveal that introducing an asymmetric hydrophobic domain into self-assembling peptoids drives the formation of a flexible bilayer composed of tightly packed amphiphilic peptoids. The flexibility of peptoid bilayers leads to the observation of assembly polymorphism. In addition, MD simulations predict the process of splitting large nanosheets into individual fibers. Both experimental results and MD simulations support the notion that the helical fiber structure is the critical intermediate for the formation of nanosheets and helical bundle structures. This work further highlights the critical role of hydrophobic interactions among amphiphilic peptoids in driving the formation of self-assembled materials with specific morphologies. Manipulating molecular interactions through peptoid side-chain chemistry provides a versatile platform for creating bioinspired materials with tailored morphologies and engineered functionalities.

RESULTS AND DISCUSSION

Design of Amphiphilic Peptoids with Asymmetric Hydrophobic Domains

In our previous studies, we reported that amphiphilic, lipid-like peptoids containing six *N*-[(4-bromophenyl) ethyl]glycine (Nbrpe) groups form membrane-mimetic nanosheets[20,21,42−46] while those containing six *N*-[(4-bromophenyl)methyl]glycine (Nbrpm) form nanotubes.[21−24,46] These studies,[5,9,15] along with related works by others,[32,47] have shown that the organized packing of peptoid hydrophobic domains is essential for stabilizing the interdigitated bilayer structure of amphiphilic peptoids, enabling the formation of distinct assembly morphologies. On the other hand, while previous experimental and computational results suggested that the formation of helical structures, nanotubes, and nanosheets could be related to each other through the peptoid bilayer structure,[43,48] controlling the polymorphism in the assembly of peptoid sequences has not been reported. For that purpose, we designed and synthesized a series of peptoids with an asymmetric hydrophobic domain composed of three alternating Nbrpe and Nbrpm groups. In contrast to aliphatic side chains,[30,49] these aromatic residues[24,32,44] are known to stabilize peptoid assemblies through enhanced hydrophobic interactions including $\pi-\pi$ interactions.[50−54] We hypothesized that the alternating Nbrpe and Nbrpm groups in the hydrophobic domain of these peptoids would generate local packing frustration[43] and facilitate the formation of a flexible bilayer structure, promoting polymorphism in peptoid assembly. All peptoids were synthesized following the previously reported submonomer solid-phase synthesis method,[21,24,30] and the detailed synthesis protocol, peptoid sequences, and peptoid characterizations and simulations are described in Supporting Methods and Figures S1−S10.

Assembly and Characterizations of Peptoid Nanostructures

To initiate peptoid assembly, lyophilized powder of $(NbrpeNbrpm)_3Nc_6$ (Figure 1a; sequence shown from C-to-N terminus) was dissolved in water and acetonitrile (v/v = 1:1) to obtain a 5.0 mM clear solution, with the solution pH at 4.0. The obtained solution was then left undisturbed at 4 °C for slow crystallization. After approximately 3 days, gel-like materials consisting of numerous peptoid assemblies were formed (see the Supporting Information for details). Atomic force microscopy (AFM) results showed that $(NbrpeNbrpm)_3Nc_6$ assembled into nanostructures, displaying a coexistence of three distinct morphologies: nanosheets (2D nanostructures), twisted ribbons (1D nanostructures with the

https://doi.org/10.1021/polymscitech.5c00123
Polym. Sci. Technol. 2026, 2, 176−185

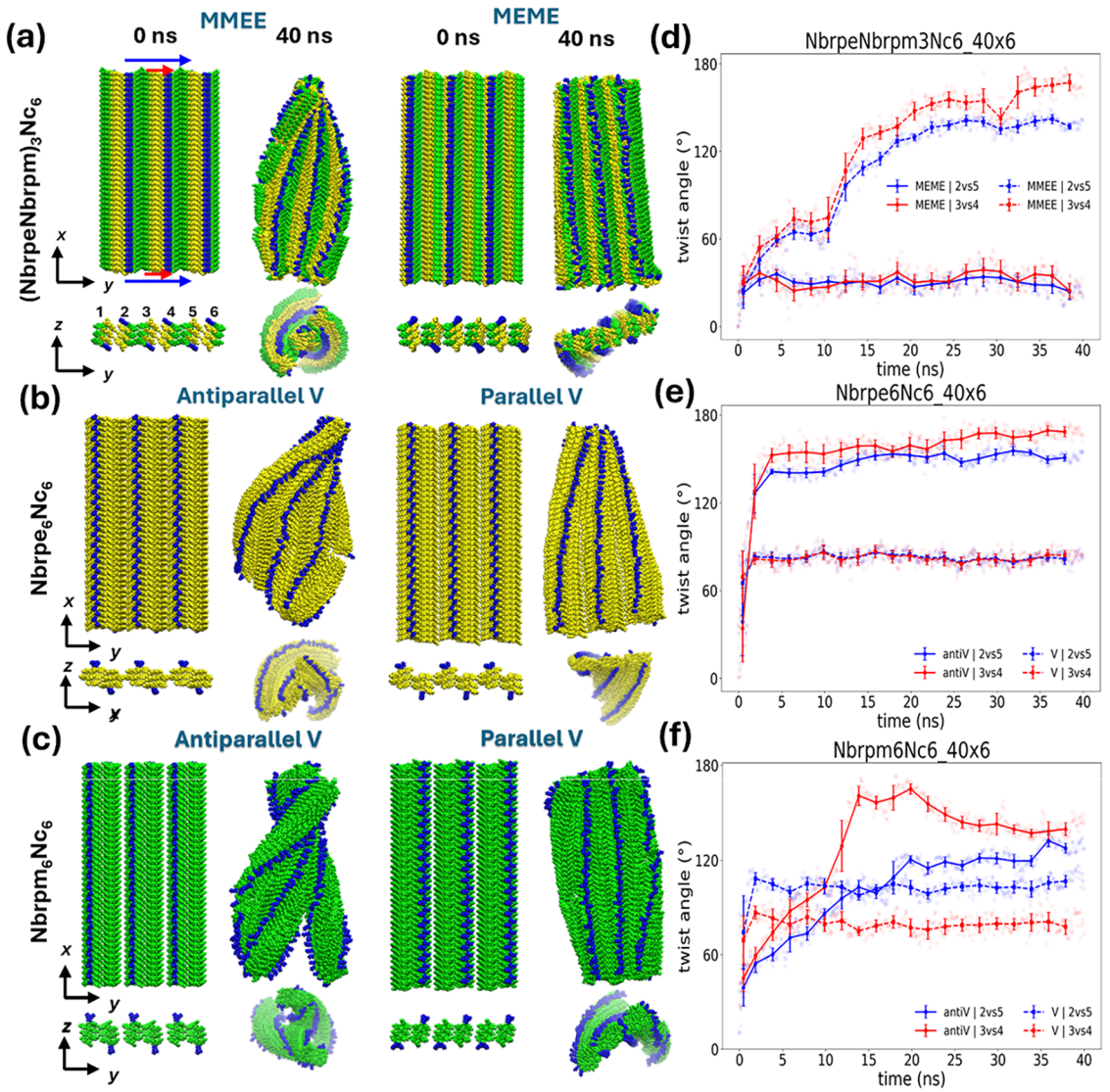

Figure 2. Molecular simulations predict the twisting of interdigitated peptoid bilayers. (a−c) Snapshots of the initial and 40 ns configurations of the bilayer structures of peptoids (a) $(NbrpeNbrpm)_3Nc_6$, (b) $Nbrpe_6Nc_6$, and (c) $Nbrpm_6Nc_6$. (d−f) Time evolution of the twisting angles of the peptoid bilayer for (d) $(NbrpeNbrpm)_3Nc_6$, (e) $Nbrpe_6Nc_6$, and (f) $Nbrpm_6Nc_6$, calculated from red (3−4) and blue (2−5) vectors at the upper and lower edges of the fibrils as illustrated in panel (a): the red vectors connect the centers of columns 3−4 on the top and bottom leaflets, while the blue vectors connect columns 2−5. Four independent runs were performed for each system and we observed consistent trends. The time evolution of the twist angles for other systems are shown in Figure S10.

width-to-height ratio larger than 10), and nanofibers (1D nanostructures with width-to-height ratio smaller than 10) (Figure 1e). AFM results showed that nanosheets and twisted ribbons have a height of approximately 2.5 nm, while nanofibers have a height of approximately 5.0 nm. Assembled $(NbrpeNbrpm)_3Nc_6$ nanosheets have a comparable height to those of $Nbrpe_6Nc_6$ (Figure S11a,b), which suggests that $(NbrpeNbrpm)_3Nc_6$ forms a similar interdigitated bilayer structure within peptoid assemblies. The coexistence of three different morphologies within $(NbrpeNbrpm)_3Nc_6$ assemblies could be due to the increased flexibility of the peptoid bilayer as a result of packed asymmetric hydrophobic domains (Figure 1b,c). To confirm the essential role of asymmetric hydrophobic side-chain packing in governing assembly polymorphism, peptoids with varying numbers of (NbrpeNbrpm) side-chain pairs were synthesized and utilized to explore their impact on assembly morphology. As shown in Figure 1d,1f, while peptoid $(NbrpeNbrpm)_4Nc_6$, with an increased number of hydrophobic side-chain pairs, assembles exclusively into nanosheet structures (Figures 1d and S12a), peptoid $(NbrpeNbrpm)_2Nc_6$, characterized by reduced hydrophobic interactions, forms helical nanofibers (Figures 1f and S12b,c). AFM results show that $(NbrpeNbrpm)_4Nc_6$ nanosheets have a height of 3.0 ± 0.3, and nanohelices of $(NbrpeNbrpm)_2Nc_6$ show heights varying from 10 to 50 nm. The height fluctuation of nanohelices indicates the multilayer stacking of helical peptoid assemblies.

To further investigate the molecular packing of these peptoids containing (NbrpeNbrpm) side-chain pairs, we performed synchrotron-based X-ray diffraction (XRD) measurements of these assembled peptoid materials. XRD results showed that the nanosheets assembled from $(NbrpeNbrpm)_4Nc_6$ exhibited the sharpest peaks, suggesting the highest crystallinity (Figure 1g). The first low-q peak (d = 3.02 nm) corresponds to the thickness of the peptoid sheet, which is consistent with the height obtained from the AFM

https://doi.org/10.1021/polymscitech.5c00123
Polym. Sci. Technol. 2026, 2, 176−185

measurement. The 1.73 nm spacing corresponds to the distance between two packed peptoid backbones along the *y*-axis with hydrophobic side chains facing each other. However, the specific molecular packing of how Nbrpe and Nbrpm face each other in that direction remains uncertain. From previous works, for the amphiphilic peptoid with six Nbrpe groups as the hydrophobic domain, the antiparallel molecular packing is dominating because the positively charged σ-holes from the covalent bond between the halogen atom and carbon could disrupt the stabilization of parallel packing and favor the antiparallel one.[32,55] Therefore, if we apply the antiparallel molecular packing to the peptoid with alternating Nbrpe and Nbrpm side chains as the asymmetric hydrophobic domain, the MMEE packing should be dominating (Figure S9). We believe this nonuniform lateral packing is crucial for the twisting and morphological changes of the assembled materials, which will be elucidated later with the help of MD simulations. The peak at 4.5 Å corresponds to the space of the alignment of peptoid chains along the *x*-axis. XRD peaks with spacings of 4.3 and 3.8 Å suggest the existence of extensive $\pi-\pi$ interactions among these Nbrpe and Nbrpm groups.[50−54] Our MD analysis (Figures S7 and S8) shows that backbone N−N, carbonyl C−C, and α-carbon (CA)−CA distances all produce broad peaks in the 3.0−4.0 Å range, with none forming a sharp ∼3.0 Å spacing; thus, the absence of a 3.0 Å reflection reflects the lack of an underlying ordered 3.0 Å backbone periodicity in these assemblies. The 3.0 Å spacing has been identified as the distance between adjacent residues along the backbone chain in the *cis*-conformation of a peptoid[42,56] (Figure S13). Compared with the peptoids having different numbers of hydrophobic groups, peptoid assemblies from those n = 4 give much sharper *d*-spacing peaks, indicating the higher crystallinity of assembled peptoid nanosheets. In contrast, the broader peaks observed for peptoid assemblies from those n = 2 or 3 suggest lower crystallinity and higher flexibility of the peptoid bilayer (Figure 1g).

To further emphasize the role of the asymmetric hydrophobic domain composed of three alternating Nbrpe and Nbrpm groups in enhancing the flexibility of the peptoid bilayer, we compared the XRD spectra of $(NbrpeNbrpm)_3Nc_6$ assemblies with those assembled from peptoids containing either six Nbrpe or Nbrpm groups (Figure S13). The similarity in their XRD spectra indicates that all of these peptoid assemblies exhibit comparable bilayer packing of amphiphilic peptoids. We then specifically analyzed the second low-q peak, which provides insights into the packing arrangement of Nbrpe and Nbrpm side chains along the *y*-direction. In this direction, the *d* spacing is 1.80 nm for nanosheets assembled from peptoids containing six Nbrpe groups,[20,21,27,42,45] while nanotubes assembled from those containing six Nbrpm groups give a *d* spacing of 1.67 nm.[24,26] The presence of a broad 1.73 nm peak in the XRD spectrum of self-assembled $(NbrpeNbrpm)_3Nc_6$ suggests a possible mixture of Nbrpe and Nbrpm groups packed in the *y*-direction (Figure S9). Such molecular packing thus leads to the high flexibility of the peptoid bilayer suitable for further twisting and folding into different morphologies.

Computational Simulation Predicts the Flexibility of Peptoid Bilayers

Experiments reveal that peptoid assemblies can adopt a range of morphologies, including flat sheets, twisted ribbons, and fibers, depending on the sequence (Figure 1). To elucidate the nonuniform lateral packing hypothesized from XRD analysis and the potential role in controlling ribbon twisting, we performed MD simulations of initially flat peptoid ribbons to assess their intrinsic stability and measure the spontaneous emergence of any inherent twisting or splitting of the ribbon. This simulation strategy builds on our previous work,[37,43] where a similar approach successfully connected molecular-level packing information to macroscopic assembly behavior.

We conducted MD simulations of three representative sequences: the polymorphic $(NbrpeNbrpm)_3Nc_6$, the focus of this work (Figure 2a); the sheet-forming $Nbrpe_6Nc6$ (Figure 2b); and the tube-forming $Nbrpm_6Nc6$ (Figure 2c), both previously reported.[43,48] Each preassembled bilayer ribbon contained six columns of 40 peptoid chains and was simulated in an explicit solvent for 40 ns. For the alternating sequence, two initial packing patterns were imposed to represent plausible registry arrangements consistent with the XRD-derived intercolumn spacing: MEME (Nbrpm−Nbrpe−Nbrpm−Nbrpe) and MMEE (Nbrpm−Nbrpm−Nbrpe−Nbrpe). The homopolymers were constructed in both parallel (V) and antiparallel (anti-V) interchain orientations to assess the influence of packing symmetry on ribbon stability. These controlled configurations allowed us to systematically probe how small variations in sequence and registry affect bilayer flexibility and the propensity for twisting. Full simulation details, including force field parameters, system construction, and MD protocols, are provided in the Supporting Information. Snapshots of the initial and 40 ns configurations are shown in Figure 2a−c. In these snapshots, Nbrpe residues are colored yellow, Nbrpm in green, and Nc6 tails in blue.

The evolution of ribbon twisting was quantified by tracking the twisting angles (θ) formed between two pairs of edge vectors: the top-edge red vector (3−4) and the bottom-edge red vector (3′−4′), and likewise between the top-edge blue vector (2−5) and the bottom-edge blue vector (2′−5′) (Figure 2a,d−f). These vectors were defined from the center-of-mass (COM) positions of the terminal monomers along each ribbon edge. Because each ribbon consists of six columns, the 3−4 pair represents the two middle columns, while 2−5 captures the second-inner pair adjacent to the center. The twist angle

$$\theta = \cos^{-1}\frac{\vec{V}_{top}\cdot\vec{V}_{bottom}}{|\vec{V}_{top}||\vec{V}_{bottom}|} \quad (1)$$

was computed over the simulation trajectory using the "*gmx gangle*" command within the Gromacs 2024.4 simulation suite.[57,58] The time evolution of θ served as a quantitative measurement of both the magnitude and spatial asymmetry of twisting across the ribbon. Mean values and standard deviations were determined using block averaging over 2 ns intervals. Comparing the evolution of 2−5 and 3−4 twisting angles helps to expose whether twisting occurs uniformly across the span of the ribbon.

The twisting-angle analysis (Figure 2d−f) reveals that both the magnitude and uniformity of ribbon twisting depend strongly on the sequence and packing pattern. For the alternating sequence $(NbrpeNbrpm)_3Nc_6$, the MMEE pattern exhibits pronounced and progressively asymmetric twisting: the red (3−4) and blue (2−5) twisting angles increase and diverge with time and reach distinct stable values, indicating uneven deformation across the ribbon width. In contrast, the MEME configuration remains relatively flat with smaller

https://doi.org/10.1021/polymscitech.5c00123
Polym. Sci. Technol. 2026, 2, 176−185

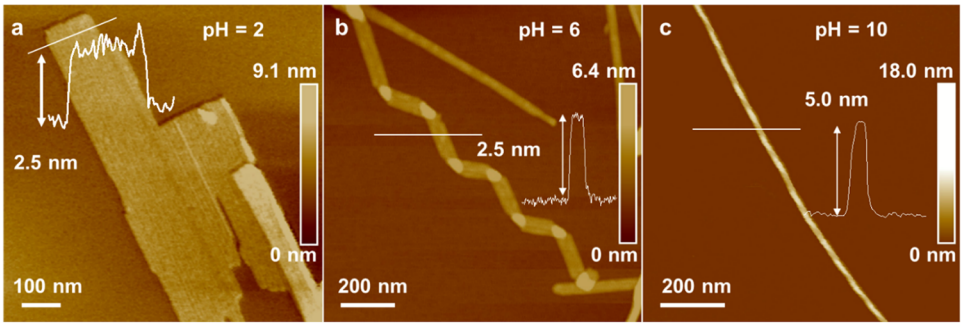

Figure 3. pH-dependent assembly of $(NbrpeNbrpm)_3Nc_6$. (a–c) AFM images showing the morphological transition at varying pH levels: (a) nanosheets at pH 2, (b) coexistence of nanosheets and nanohelices at pH 6, and (c) nanohelices at pH 10.

twisting angles and nearly overlapping red and blue traces that reflect a more symmetric morphology (Figure 2a,d). These behaviors mirror those seen in the symmetric systems, where the antiparallel V configurations of $Nbrpe_6Nc_6$ (Figure 2b,e) and $Nbrpm_6Nc_6$ (Figure 2c,f) develop larger twisting angles and evolve more slowly toward stable values, whereas the parallel V configurations remain more stable and reach their terminal twist rapidly with minimal asymmetry. For $Nbrpe_6Nc_6$ fibrils, both antiparallel and parallel V configurations showed symmetric twisting with similar angles from both peptoid pairs. Interestingly, the antiparallel V fibril of $Nbrpe_6Nc_6$ reached equilibrium within just 5 ns, much faster than that of $(NbrpeNbrpm)_3Nc_6$ fibrils. $Nbrpe_6Nc_6$ in the parallel V pattern retains a less twisted geometry.[43,48] In $Nbrpm_6Nc_6$ fibrils, the parallel fibrils also rapidly reach stable twist angles; however, an ∼15° difference in twist angles between two peptoid pairs indicates a persistent asymmetric twisting behavior consistent with its known preference to form nanotubes.[23,24,43] Finally, the $Nbrpm_6Nc_6$ antiparallel V fibril exhibited the most pronounced twisting, characterized by slow convergence of the twist angle and high asymmetry between the 2–5 and 3–4 twist angles that ultimately resulted in splitting of the fibril over the course of the simulation.

Overall, the MD simulations demonstrate that the twist angle of a preassembled ribbon, and indeed the stability of the ribbon itself, can be controlled by both the peptoid sequence and the supramolecular organization. We observe that while the MD simulations herein are designed to probe the stability of an initially flat ribbon, and that a more extensive study would be required to evaluate the relative stability of competing morphologies (e.g., extended sheets, gels, disassembled states) and probe the molecular mechanisms underpinning the full assembly pathway, the results are consistent with experimental observations of experimentally observed polymorphism and suggest how atomic-scale variations in side-chain geometry can dictate mesoscale morphology in sequence-defined peptoid assemblies. Our previous AFM and MD study[43] showed that peptoid nanosheets have bending and indentation moduli on the order of ∼1 GPa, far higher than typical lipid bilayer-like structures.[59] Yet, the alternating Nbrpe/Nbrpm hydrophobic domain introduces sufficient packing mismatch to reduce the effective bending rigidity and enable the twisting behavior observed here. In particular, the relative packing and flexibility of the Nbrpe and Nbrpm side-chain groups, stemming from the two-carbon versus one-carbon tether lengths, strongly dictate the supramolecular structure. Alternating side-chain lengths in $NbrpeNbrpm_3Nc_6$ promote twisting, whereas uniform side-chain lengths favor either flat ($Nbrpe_6Nc_6$) or symmetrically curved ($Nbrpm_6Nc_6$) assemblies. The simulation also predicts the spontaneous splitting of nanofibers in the presence of antiparallel Nbrpm packing, which suggests the potential transformation of 2D nanosheets into 1D nanostructures.

pH-Controlled Assembly of Nanosheets and Nanohelices

The molecular-level understanding of the flexibility of the $(NbrpeNbrpm)_3Nc_6$ bilayer inspired us to modulate the twisting of the peptoid bilayer and control peptoid assembly morphology by varying assembly conditions. We hypothesized that the subtle change of assembly solution pH would lead to a significant change in molecular interactions, thus leading to different assembly outcomes.[37] Here, we performed the self-assembly of $(NbrpeNbrpm)_3Nc_6$ at three different pH conditions—pH 2, pH 6, and pH 10—as the amino groups of the peptoids would be fully protonated, partially protonated, and nonprotonated, respectively,[60,61] because the pK_a of this *N*-terminal amino side chain is estimated to be around 9–10.[62] As shown from AFM and annular dark-field (ADF) scanning transmission electron microscope (STEM) images (Figures 3 and S14–S16), solution pH had a significant impact on the peptoid assembly morphologies. At pH 2, $(NbrpeNbrpm)_3Nc_6$ (Figures S14a,d and S15), with the protonated state of amino groups, assembled into nanosheets with 2.5 ± 0.3 nm in height (measured from 20 nanosheets from AFM images in Figures 3a and S14d), which is similar to the height of $Nbrpe_6Nc_6$ nanosheets with bilayer packing of amphiphilic peptoids (Figure S11).[27,48] At pH 10 (Figures 3c and S14c,f), where the amino groups remain unprotonated, AFM images revealed the formation of nanohelices with a height of 5.0 ± 0.7 nm (measured from 20 nanohelices from the AFM image in Figure S14f)—double that of peptoid nanosheets—suggesting the interdigitated bilayer stacking of $(NbrpeNbrpm)_3Nc_6$ to form nanohelices. Both left- and right-handed helices are observed (Figure S14f). Interestingly, at pH 6, the peptoid assembly results in the coexistence of nanosheets, twisted ribbons, and helical fibers (Figures 3b, S14b,e, and S16). These results further confirm that the transition between nanosheets and nanohelices can be controlled by varying the assembly solution pH. We reasoned that the protonation of amino groups led to the formation of a charged polar domain, enhancing the water solubility of peptoid molecules[62] and thereby favoring the formation of 2D nanosheets. When the amino groups of peptoids are not protonated, the reduced solubility of the polar domain makes the flat 2D nanostructure less favorable. As a result, the peptoid bilayer undergoes twisting and stacking to effectively shield the hydrophobic blocks from the aqueous

https://doi.org/10.1021/polymscitech.5c00123
Polym. Sci. Technol. 2026, 2, 176–185

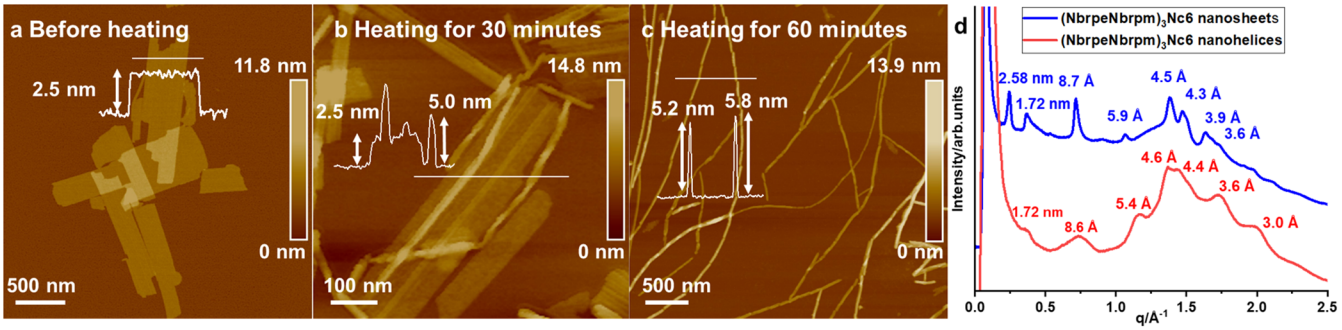

Figure 4. Morphological transition of $(NbrpeNbrpm)_3Nc_6$ assemblies from nanosheets to nanohelices induced by thermal annealing. (a) AFM image of nanosheets assembled from $(NbrpeNbrpm)_3Nc_6$. (b) AFM image showing a partial transition from nanosheets to nanohelices after 30 min of heating. (c) AFM image illustrating the complete transformation of nanosheets into nanohelices after 60 min of heating. (d) XRD spectra of the nanosheet before heating (from a) and nanohelices obtained after 60 min of thermal annealing (from panel (c)).

environment.[37] In this scenario, twisted nanoribbons and nanohelices with increased height become the preferred nanostructures.

To further validate the critical role of the peptoid polar domain in determining the assembly morphology of $(NbrpeNbrpm)_3$-containing peptoids, we designed and synthesized two additional peptoids: $(NbrpeNbrpm)_3Nc_2$ (Figure S2) and $(NbrpeNbrpm)_3$Tren (Figure S6). We then carried out the self-assembly of these peptoids under pH conditions of 2 and 10 (Figure S17). With enhanced water solubility due to the presence of three amino groups, $(NbrpeNbrpm)_3$Tren self-assembled into flat nanosheets both at pH 2 (Figure S17a) and pH 10 (Figure S17b), with a height of approximately 2.5 nm. In both cases, the polar domains of the peptoids were sufficient to shield the hydrophobic side chains from the aqueous solvent, eliminating the need for twisting or stacking of the peptoid bilayers. In contrast, $(NbrpeNbrpm)_3Nc_2$, which possesses a single amino group, exhibited self-assembly behavior similar to that of $(NbrpeNbrpm)_3Nc_6$. At pH 2, where the amino groups were protonated, it formed nanosheets with a height of approximately 2.5 nm (Figure S17c). At pH 10, $(NbrpeNbrpm)_3Nc_2$ formed helical bundles with various heights ranging from 7 to 18 nm (Figures S17d and S18), indicating that the non-protonated amino groups were insufficient to completely shield the hydrophobic side chains from the aqueous solvent in the flat bilayer form, resulting in twisting and stacking.

A similar effect was observed in the self-assembly of $(NbrpeNbrpm)_3$Dig (Figures S19 and S20) at two different solution pH levels, where the carboxyl groups exhibited varying degrees of deprotonation. As shown in Figures S19a and S20a, at pH 7, the low degree of deprotonation of carboxyl groups resulted in the formation of nanohelices with a height of 5.4 nm, reflecting the twisting of multistacked bilayers of amphiphilic peptoids. In contrast, at pH 9, the negatively charged, fully deprotonated carboxyl groups promoted the formation of nanosheets with a height of 3.2 nm (Figures S19b and S20b). Together, these findings demonstrate that the inherent flexibility of the bilayer in peptoids containing $(NbrpeNbrpm)_3$ hydrophobic domains allows for precise control over the assembly morphology by modulating the peptoid polar domains and solution pH.

Transformation of Nanosheets into Nanohelices Triggered by Thermal Annealing

Building on the flexibility of bilayers of amphiphilic peptoids containing $(NbrpeNbrpm)_3$ hydrophobic domains and the diverse assembly morphologies observed at varying solution pH, we aim to further explore the morphological transformations among these distinct nanostructures of peptoid assemblies. Herein, we opted to heat the peptoid nanosheet solution to study the morphology transformation, leveraging thermal annealing as a widely adopted technique for tuning the morphologies of supramolecular assemblies.[63] The $(NbrpeNbrpm)_3Nc_6$ nanosheets were heated at 90 °C for 30 or 60 min, and they were then cooled to room temperature. As shown in Figure 4, the nanosheets showed a clear trend to transform into nanohelices. We started with the nanosheets of $(NbrpeNbrpm)_3Nc_6$ formed at pH 2 (Figure 4a). After heating the sheet solution at 90 °C for 30 min, we observed the coexistence of nanosheets and nanohelices (Figure 4b), suggesting a partial morphological transition from sheets to helices. Interestingly, only nanohelices were observed in AFM images after the sheet solution was heated at 90 °C for 60 min (Figure 4c). A large-scale AFM image shows the coexistence of both left- and right-handed helices (Figure S21). XRD results showed that these nanosheets and nanohelices exhibit a similar bilayer packing of amphiphilic peptoids (Figure 4d). The transformation of these nanosheets into nanohelices is likely driven by the thermodynamic preference for helical twisting of peptoid bilayers over the flat sheet morphology, as this configuration more effectively shields the hydrophobic domains of peptoids from the surrounding aqueous environment.

When the heating temperature was lowered to 60 °C, the transformation of nanosheets into nanohelices significantly slowed, as shown in Figure S22a. After 60 min of heating, only a partial conversion of nanosheets into nanohelices was observed. Lowering the heating temperature further to 40 °C resulted in negligible morphological transformation, even after over 6 h of heating the nanosheet solution (Figure S22b). Such thermal annealing-induced transformation of nanosheets into nanohelices was also observed in the nanosheets assembled from $(NbrpeNbrpm)_3$Dig and $(NbrpeNbrpm)_3Nc_2$ (Figure S23). In contrast, no such transformation was observed for the nanosheets assembled from $Nbrpe_6Nc_6$ (Figure S24a), $(NbrpeNbrpm)_3$Tren (Figure S24b), and $(NbrpeNbrpm)_4Nc_6$ (Figure S24c), further highlighting the important role of peptoid bilayer flexibility in the control over assembly morphologies.

Based on our MD simulation results, which suggested that the flexibility and asymmetric packing of Nbrpm and Nbrpe side chains in peptoid bilayers may drive the splitting of

https://doi.org/10.1021/polymscitech.5c00123
Polym. Sci. Technol. 2026, 2, 176−185

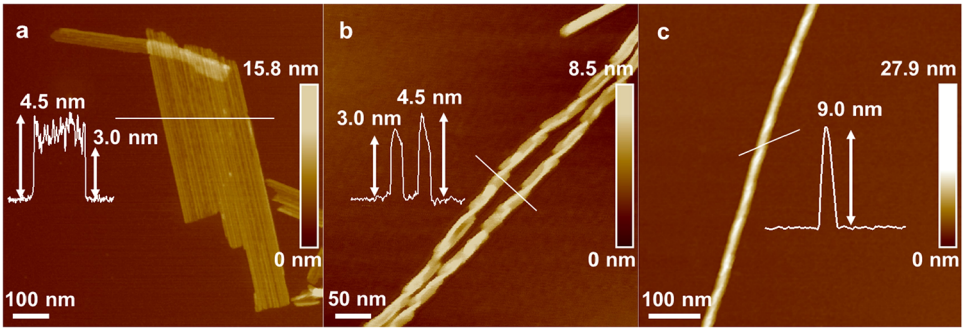

Figure 5. Representative intermediates showing the morphological transition from nanosheets to nanohelices through hierarchical processes of splitting, stacking, and twisting. (a–c) AFM images of the intermediates of peptoid assemblies during the sheet-to-helix transition; inset: height profile across the line: (a) Single-layer sheets with heights of 3 nm; (b) single-layer twisted ribbon with heights of 3 nm and the twisted part at 4.5 nm; (c) multiple-layer twisted ribbons with a height of 9 nm.

assembled nanostructures into single fibers, we further examined the time-dependent thermal annealing-induced transformation of nanosheets into nanohelices. As shown in Figure 5, time-dependent thermal heating experiments validated the transformation of nanosheets into nanofibers. Heating the nanosheets of $(NbrpeNbrpm)_3Nc_6$ at 60 °C for 1 h resulted in their transformation into parallel-packed single strands, as shown in Figure 5a. The sheets and strands had the same height of 3.0 nm, suggesting that the single strand originated from the disassembly and splitting of the nanosheets. A detailed mechanistic explanation for why the sheets break apart is beyond the scope of the present work; however, our previous theoretical modeling[43] indicates that curvature in homopolymer peptoids arises from a balance of $\pi-\pi$ stacking and interfacial energies, and for this alternating sequence, additional intercolumn side-chain mismatch may introduce packing frustration that predisposes the sheets to fragment into strands. After 3 h of heating, the parallel-packed strands split into individual strands, which subsequently began twisting into helical structures, as shown in Figure 5b. Subsequently, the single helical strands further bundled together, forming final nanohelices with heights of 9.0 nm (Figure 5c) or larger helical bundles after 6 h of heating (Figure S25). The *z*-directional stacking of helical fibers enhances the packing of aromatic motifs and effectively shields the hydrophobic domain from solvent exposure. The study of the transition from sheets to helices revealed how the increasing temperature drives the morphological transformation, first by splitting the nanosheets into single strands and subsequently facilitating the formation of helical bundles. The pitch distances of these nanohelices are nonuniform. As shown in Figure S26, the pitch distances can vary significantly even within a single helix. For example, the nanohelix depicted in Figure S26a displays pitch distance ranging from 47 to 86 nm, while another helix from the same sample, shown in Figure S26b, exhibits pitch distances ranging from 111 to 159 nm.

CONCLUSION

In summary, this study highlights the ability to control the self-assembly of synthetic peptidomimetics into diverse morphologies by tuning molecular interactions through sequence design, solution pH, and temperature. The observed polymorphism, including the coexistence of nanosheets, twisted ribbons, and nanofibers, underscores the critical role of asymmetric hydrophobic domains in enabling the flexibility of amphiphilic peptoid bilayers. Molecular dynamics simulations further reveal the mechanisms by which these domains mediate morphological transitions such as the transformation of nanosheets into nanohelices. This mechanistic understanding offers a versatile platform for designing bioinspired functional materials by linking the peptoid sequence and chemistry to specific molecular interactions and assembly behaviors. The findings pave the way for the advancement of biomimetic materials with tailored structures and functionalities.

ASSOCIATED CONTENT

Supporting Information

The Supporting Information is available free of charge at https://pubs.acs.org/doi/10.1021/polymscitech.5c00123.

Material for the peptoid synthesis, purification, and characterization of the peptoid molecules; experimental details of the peptoid assembly, pH adjustment, and thermal annealing; instrument information and sample preparation methods; molecular dynamic simulation details; and additional characterization results (PDF)

AUTHOR INFORMATION

Corresponding Author

Chun-Long Chen − *Department of Chemical Engineering, University of Washington, Seattle, Washington 98195, United States; Physical Sciences Division, Pacific Northwest National Laboratory, Richland, Washington 99352, United States;* orcid.org/0000-0002-5584-824X; Email: chunlong.chen@pnnl.gov

Authors

Renyu Zheng − *Department of Chemical Engineering, University of Washington, Seattle, Washington 98195, United States; Physical Sciences Division, Pacific Northwest National Laboratory, Richland, Washington 99352, United States*

Mingfei Zhao − *Department of Chemical and Biological Engineering, University of Alabama, Tuscaloosa, Alabama 35487, United States;* orcid.org/0000-0003-0838-5155

Wenhao Zhou − *Physical Sciences Division, Pacific Northwest National Laboratory, Richland, Washington 99352, United States; Department of Materials Science and Engineering, University of Washington, Seattle, Washington 98195, United States;* orcid.org/0009-0001-2375-4396

Thi Kim Hoang Trinh − *Physical Sciences Division, Pacific Northwest National Laboratory, Richland, Washington 99352, United States;* orcid.org/0000-0002-9906-5896
Shuai Zhang − *Physical Sciences Division, Pacific Northwest National Laboratory, Richland, Washington 99352, United States; Department of Materials Science and Engineering, University of Washington, Seattle, Washington 98195, United States;* orcid.org/0000-0003-0170-6470
James J. De Yoreo − *Physical Sciences Division, Pacific Northwest National Laboratory, Richland, Washington 99352, United States; Department of Materials Science and Engineering, University of Washington, Seattle, Washington 98195, United States;* orcid.org/0000-0002-9541-733X
Andrew L. Ferguson − *Pritzker School of Molecular Engineering and Department of Chemistry, University of Chicago, Chicago, Illinois 60637, United States;* orcid.org/0000-0002-8829-9726

Complete contact information is available at: https://pubs.acs.org/10.1021/polymscitech.5c00123

Notes

The authors declare the following competing financial interest(s): A.L.F. is a co-founder and consultant of Evozyne, Inc. and a co-author of US Patent Applications 16/887,710 and 17/642,582, US Provisional Patent Applications 62/853,919, 62/900,420, 63/314,898, 63/479,378, 63/521,617, and 63/669,836, and International Patent Applications PCT/US2020/035206, PCT/US2020/050466, and PCT/US24/10805.

■ ACKNOWLEDGMENTS

This work was supported by the US Department of Energy (DOE), Office of Science, Office of Basic Energy Sciences (BES) as part of the Energy Frontier Research Centers program: CSSAS—The Center for the Science of Synthesis Across Scales—under Award Number DE-SC0019288 [FWP 72448 at Pacific Northwest National Laboratory (PNNL)]. XRD work was conducted at the Advanced Light Source (ALS) of Lawrence Berkeley National Laboratory, which was supported by the Office of Science (No. DE-AC02-05CH11231). A portion of the AFM and S/TEM experiments were conducted at the Molecular Analysis Facility (MAF), a National Nanotechnology Coordinated Infrastructure (NNCI) site at the University of Washington, which is supported in part by funds from the National Science Foundation (Awards NNCI-2025489 and NNCI-1542101). This work was completed in part with resources provided by the University of Chicago Research Computing Center and was subsequently extended at the University of Alabama with support from the start-up fund. PNNL is multi-program national laboratory operated for DOE by Battelle under Contracts No. DE-AC05-76RL01830.

■ REFERENCES

(1) Chen, C. L.; Rosi, N. L. Peptide-based methods for the preparation of nanostructured inorganic materials. *Angew. Chem., Int. Ed.* **2010**, *49* (11), 1924−1942.
(2) Dickerson, M. B.; Sandhage, K. H.; Naik, R. R. Protein- and Peptide-Directed Syntheses of Inorganic Materials. *Chem. Rev.* **2008**, *108* (11), 4935−4978.
(3) Sommerdijk, N. A. J. M.; de With, G. Biomimetic CaCO3Mineralization using Designer Molecules and Interfaces. *Chem. Rev.* **2008**, *108* (11), 4499−4550.
(4) Meldrum, F. C.; Coelfen, H. Controlling Mineral Morphologies and Structures in Biological and Synthetic Systems. *Chem. Rev.* **2008**, *108* (11), 4332−4432.
(5) Shao, L.; Ma, J.; Prelesnik, J. L.; Zhou, Y.; Nguyen, M.; Zhao, M.; Jenekhe, S. A.; Kalinin, S. V.; Ferguson, A. L.; Pfaendtner, J.; et al. Hierarchical Materials from High Information Content Macromolecular Building Blocks: Construction, Dynamic Interventions, and Prediction. *Chem. Rev.* **2022**, *122* (24), 17397−17478.
(6) Dill, K. A.; Ozkan, S. B.; Shell, M. S.; Weikl, T. R. The protein folding problem. *Annu. Rev. Biophys.* **2008**, *37*, 289−316, DOI: 10.1146/annurev.biophys.37.092707.153558.
(7) Zhu, J.; Avakyan, N.; Kakkis, A.; Hoffnagle, A. M.; Han, K.; Li, Y.; Zhang, Z.; Choi, T. S.; Na, Y.; Yu, C.-J.; Tezcan, F. A. Protein Assembly by Design. *Chem. Rev.* **2021**, *121* (22), 13701−13796.
(8) Huang, P.-S.; Boyken, S. E.; Baker, D. The coming of age of de novo protein design. *Nature* **2016**, *537* (7620), 320−327.
(9) Li, Z.; Cai, B.; Yang, W.; Chen, C.-L. Hierarchical Nanomaterials Assembled from Peptoids and Other Sequence-Defined Synthetic Polymers. *Chem. Rev.* **2021**, *121* (22), 14031−14087.
(10) Adamcik, J.; Mezzenga, R. Amyloid Polymorphism in the Protein Folding and Aggregation Energy Landscape. *Angew. Chem., Int. Ed.* **2018**, *57* (28), 8370−8382.
(11) Jeon, H.; Han, Ar.; Oh, S.; Park, J. G.; Namkoong, M.; Bang, K. M.; Kim, H. M.; Kim, N. K.; Hwang, K. Y.; Hur, K.; et al.*et al.* Polymorphic Self-Assembly with Procedural Flexibility for Monodisperse Quaternary Protein Structures of DegQ Enzymes. *Adv. Mater.* **2024**, *36* (19), No. 2308837.
(12) Khmelinskaia, A.; Bethel, N. P.; Fatehi, F.; Mallik, B. B.; Antanasijevic, A.; Borst, A. J.; Lai, S.-H.; Chim, H. Y.; Wang, J. Y. J.; Miranda, M. C.; et al.*et al.* Local structural flexibility drives oligomorphism in computationally designed protein assemblies. *Nat. Struct. Mol. Biol.* **2025**, *32*, 1050−1060.
(13) García-Aguilar, I.; Zwaan, S.; Giomi, L. Polymorphism in tubulin assemblies: A mechanical model. *Phys. Rev. Res.* **2023**, *5* (2), No. 023093.
(14) Feiler, T.; Bhattacharya, B.; Michalchuk, A. A.; Rhim, S.-Y.; Schröder, V.; List-Kratochvil, E.; Emmerling, F. Tuning the mechanical flexibility of organic molecular crystals by polymorphism for flexible optical waveguides. *CrystEngComm* **2021**, *23* (34), 5815−5825.
(15) Cai, B.; Li, Z.; Chen, C.-L. Programming Amphiphilic Peptoid Oligomers for Hierarchical Assembly and Inorganic Crystallization. *Acc. Chem. Res.* **2021**, *54* (1), 81−91.
(16) Levin, A.; Hakala, T. A.; Schnaider, L.; Bernardes, G. J. L.; Gazit, E.; Knowles, T. P. J. Biomimetic peptide self-assembly for functional materials. *Nat. Rev. Chem.* **2020**, *4* (11), 615−634.
(17) Yang, W.; Yin, Q.; Chen, C.-L. Designing Sequence-Defined Peptoids for Biomimetic Control over Inorganic Crystallization. *Chem. Mater.* **2021**, *33* (9), 3047−3065.
(18) Gangloff, N.; Ulbricht, J.; Lorson, T.; Schlaad, H.; Luxenhofer, R. Peptoids and Polypeptoids at the Frontier of Supra- and Macromolecular Engineering. *Chem. Rev.* **2016**, *116* (4), 1753−1802.
(19) Sun, J.; Zuckermann, R. N. Peptoid polymers: a highly designable bioinspired material. *ACS Nano* **2013**, *7* (6), 4715−4732.
(20) Trinh, T. K. H.; Jin, B.; Zuckermann, R. N.; Chen, C.-L. Assembly of Metalloporphyrin Peptoids into Crystalline Nanomaterials as a Multifunctional System for Biomimetic Catalysis and Sensing. *ACS Appl. Mater. Interfaces* **2025**, *17* (31), 44347−44359.
(21) Chakma, P.; Chen, Y.; Harris, B. S.; Elhady, Y. W.; Zheng, R.; Bowden, M. E.; Shutthanandan, V.; Bard, A. B.; Trinh, T. K. H.; Zheng, X.; et al. Assembled peptoid crystalline nanomaterials as carbonic anhydrase mimics for promoted hydration and sequestration of CO2. *Nat. Commun.* **2025**, *16* (1), No. 7348.
(22) Jian, T.; Zhou, Y.; Wang, P.; Yang, W.; Mu, P.; Zhang, X.; Zhang, X.; Chen, C.-L. Highly stable and tunable peptoid/hemin enzymatic mimetics with natural peroxidase-like activities. *Nat. Commun.* **2022**, *13* (1), No. 3025.
(23) Luo, Y.; Song, Y.; Wang, M.; Jian, T.; Ding, S.; Mu, P.; Liao, Z.; Shi, Q.; Cai, X.; Jin, H.; et al. Bioinspired Peptoid Nanotubes for

Targeted Tumor Cell Imaging and Chemo-Photodynamic Therapy. *Small* **2019**, *15* (43), No. 1902485.
(24) Jin, H.; Ding, Y.-H.; Wang, M.; Song, Y.; Liao, Z.; Newcomb, C. J.; Wu, X.; Tang, X.-Q.; Li, Z.; Lin, Y.; et al. Designable and dynamic single-walled stiff nanotubes assembled from sequence-defined peptoids. *Nat. Commun.* **2018**, *9* (1), No. 270.
(25) Song, Y.; Cai, X.; Wang, M.; Du, D.; Lin, Y.; Chen, C.-L. Assembly of highly efficient aqueous light-harvesting system from sequence-defined peptoids for cytosolic microRNA detection. *Nano Res.* **2024**, *17* (2), 788−796.
(26) Li, Z.; Tran, D. K.; Nguyen, M.; Jian, T.; Yan, F.; Jenekhe, S. A.; Chen, C.-L. Amphiphilic Peptoid-Directed Assembly of Oligoanilines into Highly Crystalline Conducting Nanotubes. *Macromol. Rapid Commun.* **2022**, *43* (4), No. 2100639.
(27) Zhang, S.; Hettige, J. J.; Li, Y.; Jian, T.; Yang, W.; Yao, Y.-C.; Zheng, R.; Lin, Z.; Tao, J.; De Yoreo, J. J.; et al. Co-Assembly of Carbon Nanotube Porins into Biomimetic Peptoid Membranes. *Small* **2023**, *19* (21), No. 2206810.
(28) Kim, J. H.; Kim, S. C.; Kline, M. A.; Grzincic, E. M.; Tresca, B. W.; Cardiel, J.; Karbaschi, M.; Dehigaspitiya, D. C.; Chen, Y.; Udumula, V.; et al. Discovery of Stable and Selective Antibody Mimetics from Combinatorial Libraries of Polyvalent, Loop-Functionalized Peptoid Nanosheets. *ACS Nano* **2020**, *14* (1), 185−195.
(29) Robertson, E. J.; Battigelli, A.; Proulx, C.; Mannige, R. V.; Haxton, T. K.; Yun, L. S.; Whitelam, S.; Zuckermann, R. N. Design, Synthesis, Assembly, and Engineering of Peptoid Nanosheets. *Acc. Chem. Res.* **2016**, *49* (3), 379−389.
(30) Jin, H.; Jiao, F.; Daily, M. D.; Chen, Y.; Yan, F.; Ding, Y.-H.; Zhang, X.; Robertson, E. J.; Baer, M. D.; Chen, C.-L. Highly stable and self-repairing membrane-mimetic 2D nanomaterials assembled from lipid-like peptoids. *Nat. Commun.* **2016**, *7*, No. 12252.
(31) Jiao, F.; Chen, Y.; Jin, H.; He, P.; Chen, C.-L.; De Yoreo, J. J. Self-repair and patterning of 2D membrane-like peptoid materials. *Adv. Funct. Mater.* **2016**, *26*, 8960−8967.
(32) Xuan, S. T.; Jiang, X.; Spencer, R. K.; Li, N. K.; Prendergast, D.; Balsara, N. P.; Zuckermann, R. N. Atomic-level engineering and imaging of polypeptoid crystal lattices. *Proc. Natl. Acad. Sci. U.S.A.* **2019**, *116* (45), 22491−22499.
(33) Song, Y.; Wang, M.; Akkineni, S.; Yang, W.; Hettige, J. J.; Jin, H.; Liao, Z.; Mu, P.; Yan, F.; Baer, M.; et al. Highly Bright and Photostable Two-Dimensional Nanomaterials Assembled from Sequence-Defined Peptoids. *ACS Mater. Lett.* **2021**, *3* (4), 420−427.
(34) Wang, M.; Song, Y.; Zhang, S.; Zhang, X.; Cai, X.; Lin, Y.; De Yoreo, J. J.; Chen, C.-L. Programmable two-dimensional nanocrystals assembled from POSS-containing peptoids as efficient artificial light-harvesting systems. *Sci. Adv.* **2021**, *7* (20), No. eabg1448.
(35) Wang, M.; Song, Y.; Mu, P.; Cai, X.; Lin, Y.; Chen, C.-L. Peptoid-Based Programmable 2D Nanomaterial Sensor for Selective and Sensitive Detection of H2S in Live Cells. *ACS Appl. Bio Mater.* **2020**, *3* (9), 6039−6048.
(36) Mu, P.; Zhou, G.; Chen, C.-L. 2D nanomaterials assembled from sequence-defined molecules. *Nano-Struct. Nano-Objects* **2018**, *15*, 153−166.
(37) Zheng, R.; Zhao, M.; Du, J. S.; Sudarshan, T. R.; Zhou, Y.; Paravastu, A. K.; De Yoreo, J. J.; Ferguson, A. L.; Chen, C.-L. Assembly of short amphiphilic peptoids into nanohelices with controllable supramolecular chirality. *Nat. Commun.* **2024**, *15* (1), No. 3264.
(38) Murnen, H. K.; Rosales, A. M.; Jaworsk, J. N.; Segalman, R. A.; Zuckermann, R. N. Hierarchical self-assembly of a biomimetic diblock copolypeptoid into homochiral superhelices. *J. Am. Chem. Soc.* **2010**, *132* (45), 16112−16119.
(39) Ding, X.; Liu, D.; Jiang, X.; Chen, X.; Zuckermann, R. N.; Sun, J. Hierarchical Approach for Controlled Assembly of Branched Nanostructures from One Polymer Compound by Engineering Crystalline Domains. *ACS Nano* **2022**, *16* (7), 10470−10481.
(40) Sun, J.; Wang, Z.; Zhu, C.; Wang, M.; Shi, Z.; Wei, Y.; Fu, X.; Chen, X.; Zuckermann, R. N. Hierarchical supramolecular assembly of a single peptoid polymer into a planar nanobrush with two distinct molecular packing motifs. *Proc. Natl. Acad. Sci. U.S.A.* **2020**, *117* (50), No. 31639.
(41) Lee, Y. J.; Seidler, M.; Luo, X.; Butterfoss, G. L.; Yu, T.; Rad, B.; Xuan, S.; Zhu, C.; Prendergast, D.; Balsara, N. P.; et al. Crystalline Peptoid Nanofibers with a Single-Unit Cell Cross Section. *J. Am. Chem. Soc.* **2025**, *147* (31), 27390−27402.
(42) Trinh, T. K. H.; Jian, T.; Jin, B.; Nguyen, D.-T.; Zuckermann, R. N.; Chen, C.-L. Designed Metal-Containing Peptoid Membranes as Enzyme Mimetics for Catalytic Organophosphate Degradation. *ACS Appl. Mater. Interfaces* **2023**, *15* (44), 51191−51203.
(43) Zhao, M.; Zhang, S.; Zheng, R.; Alamdari, S.; Mundy, C. J.; Pfaendtner, J.; Pozzo, L. D.; Chen, C.-L.; De Yoreo, J. J.; Ferguson, A. L. Computational and Experimental Determination of the Properties, Structure, and Stability of Peptoid Nanosheets and Nanotubes. *Biomacromolecules* **2023**, *24* (6), 2618−2632.
(44) Hammons, J. A.; Baer, M. D.; Jian, T.; Lee, J. R. I.; Weiss, T. M.; De Yoreo, J. J.; Noy, A.; Chen, C.-L.; Van Buuren, A. Early-Stage Aggregation and Crystalline Interactions of Peptoid Nanomembranes. *J. Phys. Chem. Lett.* **2021**, *12* (26), 6126−6133.
(45) Ma, J.; Cai, B.; Zhang, S.; Jian, T.; De Yoreo, J. J.; Chen, C.-L.; Baneyx, F. Nanoparticle-Mediated Assembly of Peptoid Nanosheets Functionalized with Solid-Binding Proteins: Designing Heterostructures for Hierarchy. *Nano Lett.* **2021**, *21* (4), 1636−1642.
(46) Shao, L.; Hu, D.; Zheng, S.-L.; Trinh, T. K. H.; Zhou, W.; Wang, H.; Zong, Y.; Li, C.; Chen, C.-L. Hierarchical Self-Assembly of Multidimensional Functional Materials from Sequence-Defined Peptoids. *Angew. Chem., Int. Ed.* **2024**, *63* (24), No. e202403263.
(47) Jiang, X.; Seidler, M.; Butterfoss, G. L.; Luo, X.; Yu, T.; Xuan, S.; Prendergast, D.; Zuckermann, R. N.; Balsara, N. P. Atomic-Scale Corrugations in Crystalline Polypeptoid Nanosheets Revealed by Three-Dimensional Cryogenic Electron Microscopy. *ACS Macro Lett.* **2023**, *12* (5), 632−638.
(48) Zhao, M.; Lachowski, K. J.; Zhang, S.; Alamdari, S.; Sampath, J.; Mu, P.; Mundy, C. J.; Pfaendtner, J.; De Yoreo, J. J.; Chen, C.-L.; et al. Hierarchical Self-Assembly Pathways of Peptoid Helices and Sheets. *Biomacromolecules* **2022**, *23* (3), 992−1008.
(49) Xuan, S.; Jiang, X.; Balsara, N. P.; Zuckermann, R. N. Crystallization and self-assembly of shape-complementary sequence-defined peptoids. *Polym. Chem.* **2021**, *12* (33), 4770−4777.
(50) Chen, C. L.; Beatty, A. M. Guest inclusion and structural dynamics in 2-D hydrogen-bonded metal-organic frameworks. *J. Am. Chem. Soc.* **2008**, *130* (51), 17222−17223.
(51) Chen, C. L.; Tan, H. Y.; Yao, J. H.; Wan, Y. Q.; Su, C. Y. Disilver(I) rectangular-shaped metallacycles: X-ray crystal structure and dynamic behavior in solution. *Inorg. Chem.* **2005**, *44* (23), 8510−8520.
(52) Chen, C. L.; Goforth, A. M.; Smith, M. D.; Su, C. Y.; zur Loye, H. C. [Co-2(ppca)(2)(H2O)(V4O12)(0.5)]: A framework material exhibiting reversible shrinkage and expansion through a single-crystal-to-single-crystal transformation involving a change in the cobalt coordination environment. *Angew. Chem., Int. Ed.* **2005**, *44* (41), 6673−6677.
(53) Chen, C. L.; Su, C. Y.; Cai, Y. P.; Zhang, H. X.; Xu, A. W.; Kang, B. S.; zur Loye, H. C. Multidimensional frameworks assembled from silver(I) coordination polymers containing flexible bis-(thioquinolyl) ligands: Role of the intra- and intermolecular aromatic stacking interactions. *Inorg. Chem.* **2003**, *42* (12), 3738−3750.
(54) Chen, C. L.; Su, C. Y.; Cai, Y. P.; Zhang, H. X.; Xu, A. W.; Kang, B. S. A non-interpenetrating 2D coordination polymer from a (CH2)(8) spacer-based highly flexible linear ligand and AgCF3CO2. *New J. Chem.* **2003**, *27* (5), 790−792.
(55) Seidler, M.; Li, N. K.; Luo, X.; Xuan, S.; Zuckermann, R. N.; Balsara, N. P.; Prendergast, D.; Jiang, X. Importance of the Positively Charged σ-Hole in Crystal Engineering of Halogenated Polypeptoids. *J. Phys. Chem. B* **2022**, *126* (22), 4152−4159.
(56) Greer, D. R.; Stolberg, M. A.; Kundu, J.; Spencer, R. K.; Pascal, T.; Prendergast, D.; Balsara, N. P.; Zuckermann, R. N. Universal Relationship between Molecular Structure and Crystal Structure in

Peptoid Polymers and Prevalence of the cis Backbone Conformation. *J. Am. Chem. Soc.* **2018**, *140* (2), 827−833.
(57) Van Der Spoel, D.; Lindahl, E.; Hess, B.; Groenhof, G.; Mark, A. E.; Berendsen, H. J. C. GROMACS: Fast, flexible, and free. *J. Comput. Chem.* **2005**, *26* (16), 1701−1718.
(58) Abraham, M. J.; Murtola, T.; Schulz, R.; Páll, S.; Smith, J. C.; Hess, B.; Lindahl, E. GROMACS: High performance molecular simulations through multi-level parallelism from laptops to supercomputers. *SoftwareX* **2015**, *1-2*, 19−25.
(59) Eid, J.; Greige-Gerges, H.; Monticelli, L.; Jraij, A. Elastic moduli of lipid membranes: Reproducibility of AFM measures. *Chem. Phys. Lipids* **2021**, *234*, No. 105011.
(60) Thoma, B.; Powner, M. W. Selective Synthesis of Lysine Peptides and the Prebiotically Plausible Synthesis of Catalytically Active Diaminopropionic Acid Peptide Nitriles in Water. *J. Am. Chem. Soc.* **2023**, *145* (5), 3121−3130.
(61) Tu, Z.; Volk, M.; Shah, K.; Clerkin, K.; Liang, J. F. Constructing bioactive peptides with pH-dependent activities. *Peptides* **2009**, *30* (8), 1523−1528.
(62) Castelletto, V.; Seitsonen, J.; Tewari, K. M.; Hasan, A.; Edkins, R. M.; Ruokolainen, J.; Pandey, L. M.; Hamley, I. W.; Lau, K. H. A. Self-Assembly of Minimal Peptoid Sequences. *ACS Macro Lett.* **2020**, *9* (4), 494−499.
(63) Panja, S.; Adams, D. J. Stimuli responsive dynamic transformations in supramolecular gels. *Chem. Soc. Rev.* **2021**, *50* (8), 5165−5200.

https://doi.org/10.1021/polymscitech.5c00123
Polym. Sci. Technol. 2026, 2, 176−185